International Journal of Multidisciplinary Research and Modern Education (IJMRME)
Impact Factor: 7.315, ISSN (Online): 2454 - 6119
(www.rdmodernresearch.org) Volume 4, Issue 1, 2018

A COMPARATIVE STUDY OF MO FILMS DEPOSITED ON AISI 310 AND AL_2O_3 SURFACE USING ANODIC VACUUM ARC

Suman Choudhury* & Sanjay Kumar Sinha**
Department of Applied Physics, Birla Institute of Technology Mesra, Ranchi, Jharkhand

Cite This Article: Suman Choudhury & Sanjay Kumar Sinha, "A Comparative Study of Mo Films Deposited on AISI 310 and Al_2O_3 Surface Using Anodic Vacuum Arc", International Journal of Multidisciplinary Research and Modern Education, Volume 4, Issue 1, Page Number 146-151, 2018.

Abstract:

The Surface of Alumina and Stainless Steel was considered for thin film deposition of molybdenum by using Anodic Vacuum Arc. The evaporation was carried out at 0.07 mbar pressure and at a welding current of 60 Amperes where the temperature reached beyond 2500˚C and a thin layer of molybdenum was coated on the substrates. The corrosion rate, surface morphology, crystallite size and lattice strain were calculated by using Electrochemical Analyzer, Scanning Electron Microscope and X-Ray Diffraction respectively.

1. Introduction:

Corrosion resistance of metals have a direct impact on some of the products performance. Corrosion losses in countries with developed industry is up to 4.9% of gross national product (GNP) [1]. Protective coatings formation on metal surface relates to procedures of corrosion control. High adhesion between coating and substrate is one of the major criteria for coatings material selection. At high coating strength and low adhesion to the substrate coatings detachment and disconnection occurs. At low coating strength the bubbles with a gap appear which dramatically increases the rate of metal oxidation [2]. Definitely, there are other problems in relevance to protective coatings application which we have not considered. Qualitative methods of corrosion evaluation include electrical test. Electrochemical analysis (ECA) was used for corrosion rate investigation of polycystalline coatings (e.g. molybdenum coatings) deposited by anodic vacuum arc. Scientific and practical interest of thin molybdenum coatings formation is caused by its heat resistance, high mechanical strength and unique electrical properties. Molybdenum is used as a material for the manufacture of contact groups and protective layers in integrated circuits [3], thin film solar cells [4, 5], superconducting thin films [6] and optical interference coatings [7].

2. Experimental:

A. Materials:

Two types of substrates were used throughout the experiments. Specimens were prepared with different dimensions.

- ✓ Stainless Steel Substrate, *Dimension:*- 1.5 cm × 1.5 cm
- ✓ Alumina Substrate, *Dimension:*- 1 cm diameter circular substrate

Commercially available polycrystalline α-Al2O3 (Alumina) of thickness 1mm was used for study. Also, commercial grade of AISI 310 Austenite stainless steel sheets of 15 mm thickness was considered for the present study. AISI 310 is a type of biomaterial used in medicine practises [8]. The chemical composition of the steel is given in Table 1.

Elements	C	Ni	N	Cr	S	P	Mn	Si	Fe
Composition	0.075	20.1	0.05	24.4	0.023	0.045	1.91	1.60	Balance

Table 1: Chemical composition (wt%) of AISI 310 [9]

B. Polishing Machine:

The substrates were cleaned and prepared before deposition. Substrates were subjected to ultrasonic bath with acetone using an Oscar Ultrasonic Cleaner.

C. Anodic Vacuum Arc Deposition System:

Anodic arc proposes an energetic source for producing thin films. In AVA, the cathode operates in spot mode while the hot evaporating anode provides the evaporating material [10]. The schematic diagram of the AVA deposition system is shown in figure 1. AVA is a source of pure metal vapor plasma free from macroparticles that offers various advantages over other deposition techniques like, high deposition rates, low thermal load on the substrate, and high degree of ionization [11, 12]. Flux ionization can be varied significantly from 1% to 30% while ion energies range from 2 eV to 150 eV offering a better control over the deposition process [13]. Deposition rate up to 40 nm/s can be achieved with input power in the range of 400W to 900W, which is much higher than those obtained by using other different physical vapor deposition processes. The high deposition rate (5 to 40 nm/s) of AVA coupled with macroparticle free stream of ionized energetic particles

makes it industrially viable. Unlike cathodic arcs, anodic arcs are sustained by the material evaporated from the anode.

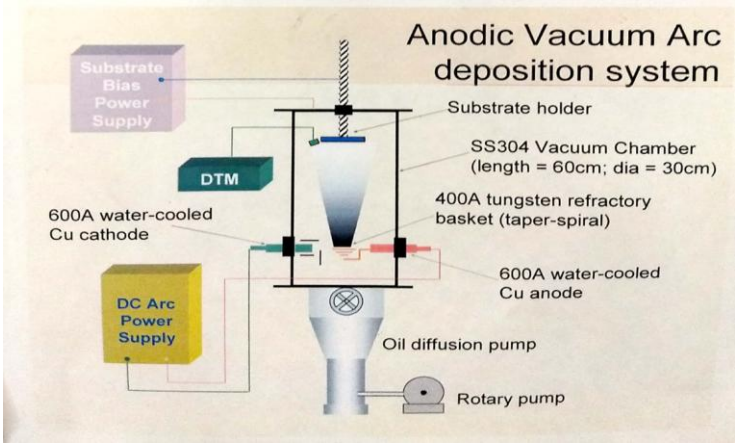

Figure 1: A Schematic diagram of AVA chamber [10]

In AVA, the cathode is either completely inactive or has many rapidly moving spots on the cathode surface. All of the components that sustains the arc is provided by the anode. With respect to coating, this source combines the advantages of thermal evaporation, i.e., high evaporation rates, low thermal load to a substrate, low voltage operation, and inexpensive equipment, with the advantages of plasma-supported processes, i.e., condensation from the plasma state resulting in well adherent coatings of compact structure. The high degree of ionization provides the basis for the manipulation of the ion energy with the help of bias voltages to produce coatings meeting specific requirements. In contrast to other plasma-supported coating processes, anodic arc evaporation operates without a discharge-sustaining gaseous atmosphere. This feature is of advantage in many applications where coatings free from an incorporated gas are desired. On the other hand, the arc source can be operated in an ambient gas atmosphere below a pressure of 1 Pa [10]. Thus, there exists an additional facility to produce reactive coatings. Moreover, the anodic arc produces films that are of very high quality and do not suffer from macroparticle inclusions.

D. X-Ray Diffraction (XRD):

The X-ray diffraction profiles of our samples were recorded with a Rigaku Smart Lab diffractometer using Photon Max high-flux 9 kW rotating anode X-ray source coupled with a HyPix-3000 high-energy-resolution 2D multidimensional semiconductor detector. The diffractometer uses Cu-Kα radiation (wavelength of about 1.54 Å). Small crystallite size and crystal imperfection or defects (vacancies, dislocations, grain boundaries and voids) are commonly considered to be a reason for broadening of diffraction peaks.

E. Electrochemical Analyzer (ECA):

The basic principle of corrosion is the formation of electrolyte due to thin film of moisture on a metal surface for atmospheric corrosion. Although most corrosion takes place in water, corrosion in non-aqueous systems is also known. Because corrosion occurs via electrochemical reactions, electrochemical techniques are ideal for the study of the corrosion processes. The corrosion resistance of material is an important factor in determining its biocompatibility. Every implant material corrodes inside the human body. Different materials have different intrinsic aptitudes to corrode. The more noble the material, the lesser is its aptitude to corrode. Corrosion resistance of all of our samples were studied using Electrochemical Analyzer (ECA), model 660 Series, CHI Instruments, made in USA, located at BIT Mesra, Ranchi. For corrosion analysis, samples were immersed in Ringer solution (2.1 gm NaCl in 50 ml of distilled water; 3.5 wt% NaCl). Additional electrodes, counter electrode & saturated calomel electrodes are immersed in the solution, and all the electrodes are connected to a device called a potentiostat. A potentiostat acknowledges the variation of potential of the sample in a controlled manner and measures the current ow as a function of potential.

F. Scanning Electron Microscope (SEM):

Surface topography and overview pictures of the coated substrates were collected in the scanning electron microscope JEOL JSM-6390LV model. The tungsten filament of SEM utilizes a tilting and rotating mechanical stage. It incorporates low vacuum back-scattered electron imaging for acquisition of high-resolution images of non-conductive, unprocessed samples. Secondary electrons were used for topographic investigations of the surface. Before the analysis, treated substrates were briefly coated with platinum for better vision and contrasting images.

3. Results and Discussions:

I. X-Ray Diffraction Analysis:

XRD was used to determine the crystallite size of the coatings. Broadening of diffraction peaks arises mainly due to two factors: small crystallite size and lattice strain. These factors transform a perfect peak (peak without width) into an observed broadened peak. The diffraction pattern is given for two prepared samples.

We have compared the patterns through PCPDFWIN database.

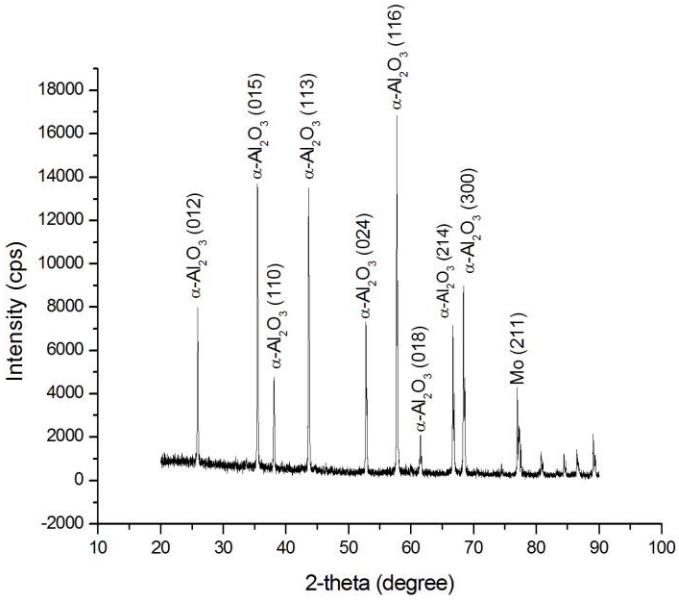

(a)

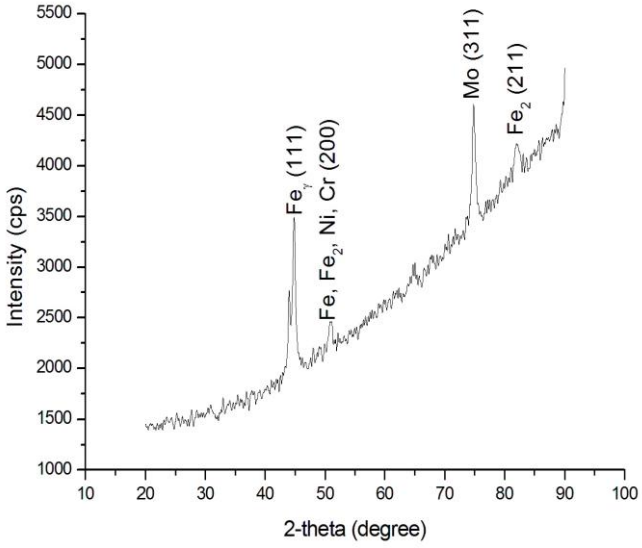

(b)

Figure 2: XRD plot for Molybdenum coating on (a) Alumina Substrate & (b) Stainless Steel Substrate

(a) Sample 1: Mo Coated on Alumina Substrate

The peaks at intensities (8083.9, 13964, 5026.3, 13661,7661.9, 17123, 2220, 7423.1, 9024.63) (cps) indicates the presence of α-Al2O3. The most interesting peak is at the intensity 4420.20 cps corresponding 2-theta value of 77.01 degree which have a Miller Indice of (211). This peak signifies the presence of Molybdenum. The crystallite size was determined to be 71.6 nm and the lattice strain was found to be 0.0015 respectively.

(b) Sample II: Mo Coated on Stainless Steel Substrate

The diffraction pattern had two major peaks i.e.; at the intensity (cps) of 765.24 and 684.67 with corresponding 2-theta value of 44.855 degree and 74.77 degree respectively. Similar patterns with peaks indicating the presence of Fe, Fe_2, Cr, Ni and such elements had been observed [14]. The peak at the angle 74.7745 degree indicates the presence of Mo ensuring the evidence that Molybdenum is coated on the surface of Stainless Steel featuring the reflecting plane as the (311) plane. The crystallite size was found to be 21.83 nm and the lattice strain is 0.0052.

II. Electrochemical Analysis:

The corrosion rate per unit area of a material is expressed as a current density since the weight loss of a metal from a given area is proportional to the current density. The temperature of the solution during the measurement was kept constant at 37.6±1˚C. The corrosion current (I_C) and corrosion rate (C_R) was determined using the software provided with the system.

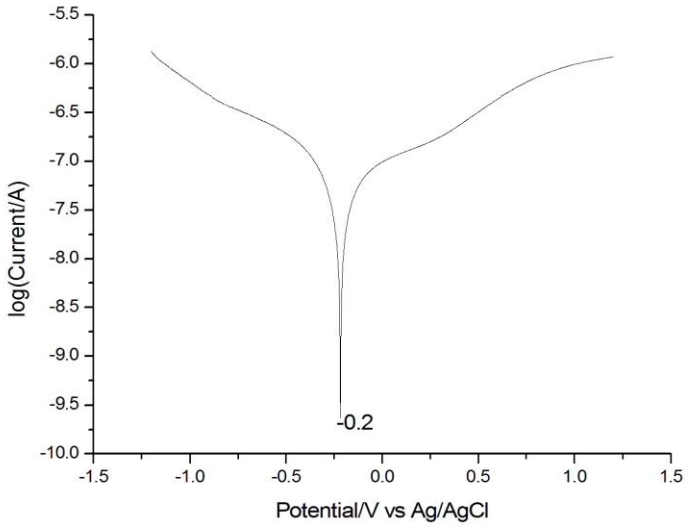

(a)

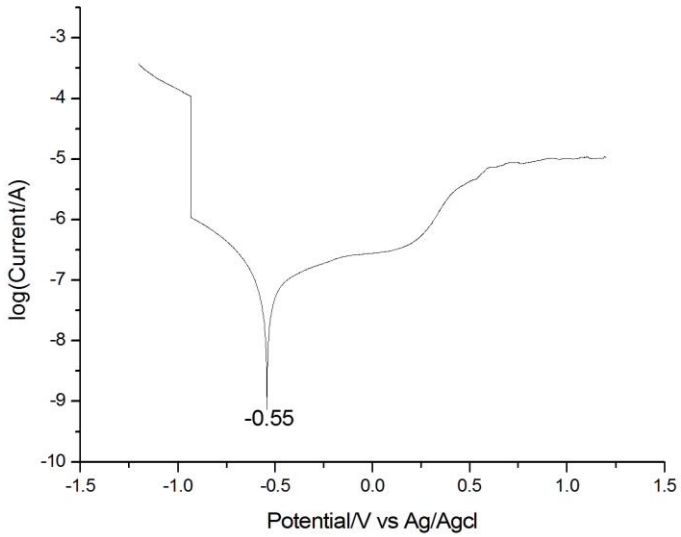

(b)

Figure 3: Tafel plot for Molybdenum coating on (a) Alumina & (b) Stainless Steel

The Tafel plot determines some specific parameters for the coatings such as the corrosion current and the corrosion rate. From Tafel Plots figure 4 & 5 the corrosion rate of coated Stainless steel and Alumina was found to be 1.408×10^{-2} mil/year and 3.281×10^{-2} mil/year. From Table 2, the Corrosion rate of Molybdenum coated on Stainless Steel substrate was found to be much lower than the coated Alumina substrate. So, we can conclude that this type of coating can benefit various applications like in furnaces or in industrial applications etc.

Substrates	**Cathodic Tafel Slope**	**Anodic Tafel Slope**	**Corrosion Current (I_C) Amperes**	**Corrosion Rate(C_R) (mil/year)**	**Corrosion Rate(C_R) (Angs/min)**
Coated Alumina	4.09	3.158	4.157×10^{-8}	3.281×10^{-2}	1.568×10^{-2}
Coated SS	4.963	2.568	7.789×10^{-8}	1.408×10^{-2}	6.806×10^{-3}

Table 2: Shows the specific corrosion characteristics of the substrates after deposition

III. Scanning Electron Microscope Analysis:

Porosity is visible in the provided images, considered to be as defects. SEM images figure 8 & 9 indicates thin film formation on the Alumina Substrate where grain size was bigger than 10 µm. Similarly, figure 6 & 7 shows thin film deposition on the SS substrate where grain size was bigger than 10 µm (21.83 nm to be exact).

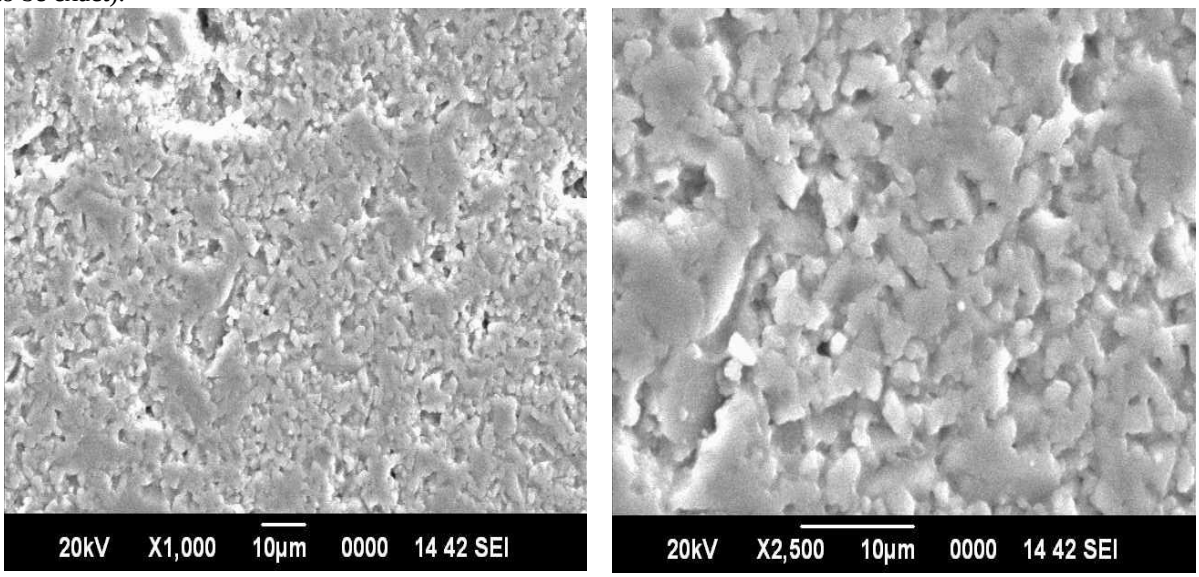

(a) (b)

Figure 4: SEM images from investigation of coated Alumina surface at a magnification of (a) 1000 & (b) 2500

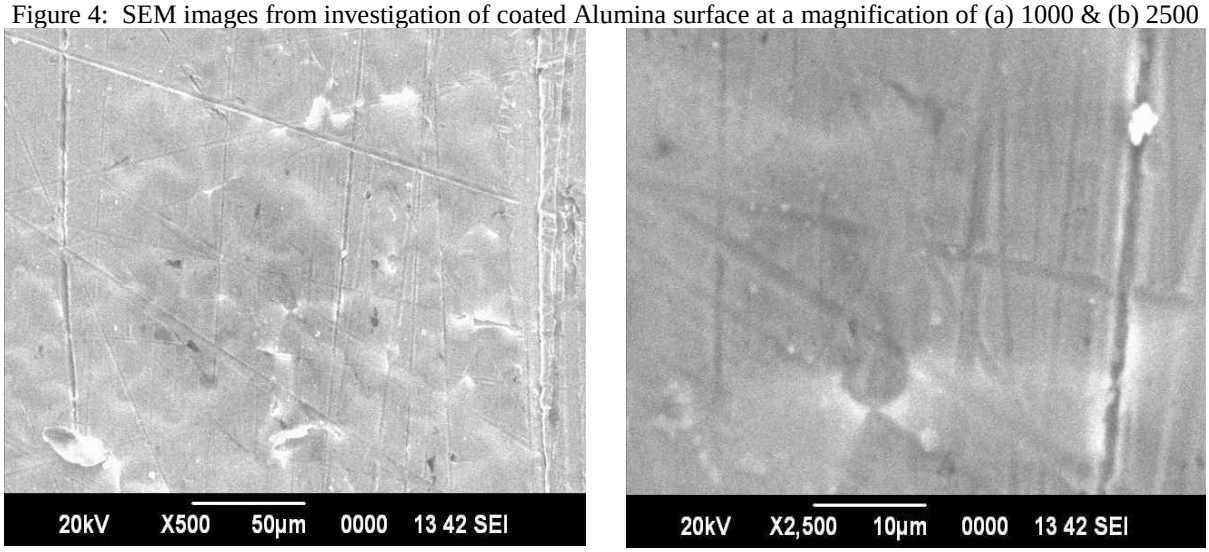

Figure 5: SEM images from investigation of coated Stainless Steel surface at a magnification of (a) 500 & (b) 2500

A higher magnification image makes the picture clear i.e; at a magnification of ×2,500 showing the morphology, crystallites and proof of non-uniform deposition. The given SEM images clearly indicated that our thin film have polycrystalline crystal structure and hence can be used for typical solar cell construction with good efficiency.

The scratched lines visible in figure 6 & 7 were due to mechanical polishing of the substrates. Also, the thin grains formation visible at figure 6 and at the edge of figure 8 clearly indicates that the thin film formation was non-uniform which is usual in thermal evaporation techniques. Alternatively, we can also use RF Magnetron Sputtering deposition technique for better adhesiveness but with high macroparticle inclusion.

4. Conclusion:

The deposition of Molybdenum on various substrate such as Alumina and Stainless Steel was carried out by using the Anodic Vacuum Arc system and compared with respect to their structural and corrosive properties. AVA deposition rate is much higher than that of sputter deposited materials. High deposition rate at large distances from the anode or cathode surface is an important advantage of AVA over other deposition techniques. However, the film depositions were found to be non-uniform in nature as seen through SEM. Hence, sputtering methods were more effective then thermal evaporation methods in relevance to adhesive and

uniformity traits. The surface morphological studies reveal that films have pores. The corresponding Mo films possess smaller grains. The Corrosion rate of Molybdenum coated on Alumina and Stainless Steel substrate were compared. Hence, we can conclude that this type of coatings can be beneficiary for various applications like bulletproof glass, in furnaces, industries etc. In the future, Molybdenum deposition on different types of substrates can increase certain characteristics such as corrosion resistance and in some case biocompatibility. Substrates with high melting point and higher nanohardness can be used like Titanium or Aluminium alloys. Meanwhile evaporation boat with high melting point and pure metal composition could minimize impurity in thin films if deposited by thermal evaporation methods.

5. Acknowledgement:

This work was carried out with support of Mr Raj Kishore Pramanik who was responsible for the operation of Anodic Vacuum Arc (AVA) deposition system stationed in Plasma Laboratory, and the Central Instrumentation Facility (CIF) of BIT Mesra, Ranchi, India

6. References:

1. Thompson, N. G., Yunovich, M., & Dunmire, D. (2007). Cost of corrosion and corrosion maintenance strategies. Corrosion Reviews, 25(3-4), 247-262.
2. Blesman, A. I., Postnikov, D. V., Polonyankin, D. A., Teplouhov, A. A., Tyukin, A. V., & Tkachenko, E. A. (2017, June). Molybdenum protective coatings adhesion to steel substrate. In Journal of Physics: Conference Series (Vol. 858, No. 1, p. 012003). IOP Publishing.
3. Klabunde, F., Löhmann, M., Bläsing, J., & Drüsedau, T. (1996). The influence of argon pressure on the structure of sputtered molybdenum: From porous amorphous to a new type of highly textured film. Journal of applied physics, 80(11), 6266-6273.
4. Ashrafee, T., Aryal, K., Rajan, G., Karki, S., Ranjan, V., Rockett, A., ... & Marsillac, S. (2015, June). Effect of substrate temperature on sputtered molybdenum film as a back contact for Cu (In, Ga) Se2 solar cells. In Photovoltaic Specialist Conference (PVSC), 2015 IEEE 42nd (pp. 1-5). IEEE.
5. Liu, X., Cui, H., Kong, C., Hao, X., Huang, Y., Liu, F., ... & Green, M. (2015). Rapid thermal annealed Molybdenum back contact for Cu2ZnSnS4 thin film solar cells. Applied Physics Letters, 106(13), 131110.
6. Andreone, A., Barone, A., Di Chiara, A., Mascolo, G., Palmieri, V., Peluso, G., & Di Uccio, U. S. (1989). Mo-Re superconducting thin films by single target magnetron sputtering. IEEE Transactions on Magnetics, 25(2), 1972-1975.
7. Jakubiak, R., Murphy, N., Sun, L., Grant, J., & Jones, J. (2013, June). Deposition of Metallic and Dielectric Molybdenum Films via Modulated Pulse Power Magnetron Sputtering. In Optical Interference Coatings (pp. FC-5). Optical Society of America.
8. Minciuna, M. G., Vizureanu, P., Abdullah, M. M. B., Achitei, D. C., Istrate, B., Cimpoesu, R., & Focsaneanu, S. C. (2017, June). Surface Characterization of New Biomaterials. In IOP Conference Series: Materials Science and Engineering (Vol. 209, No. 1, p. 012022). IOP Publishing.
9. Singh, P. K., Kumar, A., Sinha, S. K., Aggarwal, A., & Singh, G. P. (2017). Enhancement of surface properties of nanocrystalline TiN coated plasma nitrided AISI 310 austenitic stainless steel. International Journal of Surface Science and Engineering, 11(6), 547-562.
10. Mukherjee, S. K., Joshi, L., & Barhai, P. K. (2011). A comparative study of nanocrystalline Cu film deposited using anodic vacuum arc and dc magnetron sputtering. Surface and Coatings Technology, 205(19), 4582-4595.
11. Sinha, M. K., Mukherjee, S. K., Pathak, B., Paul, R. K., & Barhai, P. K. (2006). Effect of deposition process parameters on resistivity of metal and alloy films deposited using anodic vacuum arc technique. Thin Solid Films, 515(4), 1753-1757.
12. Ehrich, H., Hasse, B., Mausbach, M., & Müller, K. G. (1990). The anodic vacuum arc and its application to coating. Journal of Vacuum Science & Technology A: Vacuum, Surfaces, and Films, 8(3), 2160-2164.
13. Mausbach, M., Ehrich, H., & Müller, K. G. (1993). Properties of thin copper films, condensed from a copper plasma with ion energies between 2 and 150 eV. Journal of Vacuum Science & Technology B: Microelectronics and Nanometer Structures Processing, Measurement, and Phenomena, 11(5), 1909-1915.
14. Gunes, I., & Yıldız, I. (2016). Investigation of Adhesion and Tribological Behavior of Borided AISI 310 Stainless Steel. Matéria (Rio de Janeiro), 21(1), 61-71.